Available online at www.sciencedirect.com
ScienceDirect
Journal of Geometry and Physics 57 (2007) 745–764
JOURNAL OF GEOMETRY AND PHYSICS
www.elsevier.com/locate/jgp

The discrete $SU(3)$ transform and its continuous extension for triangular lattices

A. Atoyan*, J. Patera

Centre de Recherches Mathématiques, Université de Montréal, C.P. 6128, succursale centre-ville, Montréal (Québec) H3C 3J7, Canada

Received 18 June 2005; received in revised form 25 April 2006; accepted 25 May 2006
Available online 12 July 2006

Abstract

We develop a new method for the discrete Fourier-type transform of multi-dimensional grid functions, which is based on orbit functions of compact Lie groups of different symmetries. Here we present an implementation of this transform, abbreviated here as DOFT (for *Discrete Orbit Function Transform*), for a 2-dimensional discrete function $\{f_{k,m}\}$ produced by sampling of a continuous function $f(z)$ with $z \in \mathbb{R}^2$ on the points $z_{k,m}$ of an equilateral triangular grid F_N with N equal subintervals along each of its edges. The DOFT for such a triangular grid corresponds to implementation of the case of Lie group $SU(3)$. We present the mathematical details for realization of this case, and show that the method provides an exact solution to the problem of the discrete Fourier-type transform for such symmetry grids. In this paper we also continue development of the approach of generalization of a discrete inverse transform to the form of a continuous trigonometric polynomial. We describe and exemplify the properties of such a *continuous extension* of the DOFT (abbreviated as CEDOFT) for the $SU(3)$ group, which proves an effective tool for interpolation of the discrete function onto all points of the triangular region F. Like in the case of the CEDOFT on $SU(2)$ studied in detail earlier, the CEDOFT on $SU(3)$ has very good properties of convergence with the increase of N. It also shows localization and differentiation properties, which can be useful for a number of practical applications.

Keywords: Lie groups; Triangular lattice; Discrete transforms; Trigonometric polynomial; Interpolation

1. Introduction

Numerical computation of various transforms is being widely implemented in practical science and industry, and it also attracts significant theoretical research (e.g. see [7,28,27]). Our contribution here can be viewed from 4 different perspectives:

(I) Here we present mathematical details for a specific type of discrete transform that we used earlier in [4] to suggest a new method for signal processing in ground-based gamma-ray astronomy.

(II) It is a 2-dimensional implementation of the discrete Fourier (or Fourier-*type*) transforms on compact semisimple Lie groups, the transform bases of which are given by orbit functions of the group [15,16,10,11]. Note that the "orbit functions" considered in those references, as well as in this paper, are the C-functions of [21].

* Corresponding author. Tel.: +1 514 343 6111; fax: +1 514 343 2254.
E-mail address: atoyan@crm.umontreal.ca (A. Atoyan).

0393-0440/$ - see front matter
doi:10.1016/j.geomphys.2006.05.008

For simplicity, we abbreviate these transforms as DOFT standing for "discrete orbit function transforms". The 1-dimensional analog, that corresponds to the group $SU(2)$, is reduced to the transform known otherwise as the discrete cosine transform (DCT) [1,26], which has been studied in detail in our recent work [3]. The case here corresponds to a different underlying group, which is the compact simple Lie group $SU(3)$.

(III) It is a discrete transform on an equilateral triangular grid, which is the basis for the hexagonal grid. It is efficient, versatile, and easily implementable in practice, once the technical tools worked out here are available. It compares favorably with the earlier set-up of hexagonal transforms (see for example [14] and references therein).

(IV) It is a particular case of a vastly more general approach [16,21,11] to discrete transforms on Lie groups in any dimension $1 \leq n < \infty$. Here n coincides with the rank of the underlying Lie group (e.g. see [9,12,13] for the group E8). For 2 groups of the same rank the implementations are different from the viewpoint of symmetries of discrete n-dimensional grids involved. The case of SU(3) is one of the 4 possibilities for the rank $n = 2$. The case of $SU(2) \times SU(2)$ corresponds to grids with rectangular symmetry. It has been considered in the context of multi-dimensional generalizations of the DCT in [3,23]. Possible applications of this DOFT in the areas of data processing and imaging have been discussed in [5,6]. The remaining cases are the groups $O(5)$ and $G(2)$, the group theoretical bases of which transforms are considered separately in [23,24] in conjunction with the groups $SU(2) \times SU(2)$ and $SU(3)$, respectively. They also realize cases of triangular grids, but of different symmetries than the equilateral triangle in the case of SU(3). The SU(3) transform is distinguished from all those DOFTs also in the sense that it is the only case where the transform basis is given by sets of complex-valued orbit functions. The 2-dimensional analogs of these cosine transforms in the sine bases are developed in [25].

There is another new idea pursued here, as compared with the common discrete transform practice. It is the *continuous extension* (hereafter, CE) of the discrete transform. As an idea it seems quite natural to put a continuous trigonometric polynomial function into correspondence with the discrete transform. For many years, however, the properties of such an extension in the case of the discrete Fourier transform (hereafter DFT) have not been clearly discussed in the literature. A tacit 'common wisdom' in that regard was that one has to 'take care' of the high-frequency harmonics of the DFT, and that DFT is "a Fourier representation of a finite sequence... rather than a continuous function" (see [19], p. 87). We have shown in [3], in the context of DCT, which is the DOFT of the $SU(2)$ group, that it is quite different in the case of continuous extensions of the DOFT, hereafter abbreviated as CEDOFT.[1] This conclusion is further supported by the results presented here for the case of the $SU(3)$ group.

In Section 2 the mathematical tools are recalled because the case of $SU(3)$ is technically rather different from the simplest case considered in [3]. In this section, the general problem is first set up in the fundamental region (an *equilateral triangle* in this case) of the maximal torus of $SU(3)$. Then the new expansion functions, called *orbit functions*, on which our method is based, are explicitly described here, and their symmetries are shown.

In Section 3 we describe the $SU(3)$-transform on an equilateral triangular grid. Our main goal is summarized in Eqs. (59) and (41). Crucial is the operation of the sesquilinear product of functions (42) on the triangular grid. For its versatility, it is indispensable that the grid is group-theoretically defined through the set of its elements of any given *finite order* N. Indeed, without that it would be rather problematic to guess the values, or even the presence, of coefficients denoted as $P_{k,m}$ and required for the discrete orthogonality property (54) of orbit functions [15,16]. In addition, we also show here that even the halves of the orbit functions of $SU(3)$ (2 triplets connected to each other through a single reflection operator) are also discretely orthogonal on the grids. Points of the triangular grid turn out to be in one-to-one correspondence with elements of a finite Abelian group on the maximal torus of $SU(3)$. The fact that there is an unlimited number of such groups in the torus provides the option of choosing uniform grids of any density.

Properties of the CEDOFT function $\phi_N(z)$ are described in Section 4. The first one is the *convergence* of the interpolation provided by $\phi_N(z)$ between grid points, while retaining the exactness of the discrete transform at the points of the grid F_N (with N subdivisions along each side of the equilateral triangle). A continuous model function $f(z)$ is chosen and sampled on the grid F_N, producing the digital data $f_{k,m} \equiv f(z_{k,m})$ for our transform. Continuous extension $\phi_N(z)$ of the transform is then compared with $f(z)$. The denser the grid, the more closely $\phi_N(z)$ resembles $f(z)$; at the grid points they coincide by construction. We also show that even the approximation of discrete functions

[1] Note that in [3,5,6,2] we have used the acronyms DGT (standing for "discrete group transform") and CEDGT, instead of DOFT and CEDOFT used here; we believe the new acronyms more clearly specify these transforms.

by a modified CEDOFT series produced by truncation of high-order harmonics converges well and can be useful for removing the noise from the discrete data.

The second important feature of CEDOFT is the *localization* property. It ensures small (diminishing) local influence of relatively distant perturbations with increasing density of the grid points. We will formulate the *localization principle* for the CEDOFT and exemplify its impact by numerical computation. The convergence of $\phi_N(z)$ is fast, such that also in the case of $SU(3)$ the CEDOFT provides a *smooth* interpolation to the original function $f(z)$, which is 'differentiable' in the sense that $\lim_{N\to\infty}(\mathrm{d}\phi_N/\mathrm{d}z) = \mathrm{d}f/\mathrm{d}z$. A detailed proof of these properties in the case of $SU(2)$ and its multi-dimensional implementations is given in [3].

2. Mathematical preliminaries

2.1. Functions on the fundamental region of $SU(3)$

The compact simple Lie group $SU(3)$ can be faithfully presented as the group of all unitary matrices of size 3×3 with determinant equal to 1. Two elements $h, h' \in SU(3)$ are conjugate if there is an element $h_0 \in SU(3)$ such that $h' = h_0 h h_0^{-1}$. All elements which are mutually conjugate form one conjugacy class of $SU(3)$. There are infinitely many conjugacy classes in the group. If an element g is of finite order, i.e. $h^K = 1$ for some integer K, then all of its conjugacy class consists of elements of the same order.

The subjects of interest to us are functions f of conjugacy classes of $SU(3)$, also called class functions, i.e. such that

$$f(h) = f(h_0 h h_0^{-1}), \quad \text{for all } h, h_0 \in SU(3).$$

Any unitary matrix can be diagonalized by a unitary transformation. Therefore every element of $SU(3)$ is conjugate to at least one diagonal matrix in the defining 3-dimensional representation.

The diagonal matrices of $SU(3)$ form a maximal torus T of $SU(3)$. Furthermore, all maximal tori are $SU(3)$-conjugate, hence we can put:

$$\mathsf{T} = \left\{ h(x,y,z) = \begin{pmatrix} \mathrm{e}^{2\pi \mathrm{i} x} & 0 & 0 \\ 0 & \mathrm{e}^{2\pi \mathrm{i} y} & 0 \\ 0 & 0 & \mathrm{e}^{2\pi \mathrm{i} z} \end{pmatrix} \middle| \, x + y + z = 0 \right\}. \tag{1}$$

Note that $h(x, y, z)$ and $h(x + a, y + b, z + c)$ represent the same element in T if $a, b, c \in \mathbb{Z}$, simply because for integers the exponents $\mathrm{e}^{2\pi \mathrm{i} a}$ etc. are equal to 1. The condition $x + y + z = 0$ in (1) gives the equation of a plane called the defining plane. Within that plane one fixes a region F whose points are in one-to-one correspondence with the conjugacy classes of elements of $SU(3)$. Then it is convenient to consider the class functions f to be the functions defined on F.

Although F can be chosen and parametrized in many ways, it is advantageous to follow the practice in Lie theory. The advantages are twofold: (i) the $SU(3)$ case becomes a special case of any semisimple compact Lie group, and (ii) one gets technically the simplest description possible. The price to pay for that is the need to work with two non-orthogonal bases simultaneously, the so called α- and ω-bases.

Let $\mathbb{R}^2$ be the real Euclidean plane containing F. The standard parametrization of the defining plane makes F an equilateral triangle with vertices (0, 0), (1, 0), and (0, 1) relative to the ω-basis. The vectors

$$\omega_1 = (1, 0), \quad \omega_2 = (0, 1), \quad \text{where } \measuredangle\{\omega_1, \omega_2\} = 60^\circ,$$

are called the fundamental weights of $SU(3)$ (see Fig. 1). Elements $z = a\omega_1 + b\omega_2$ of the fundamental region F can now be described explicitly:

$$F = \{a\omega_1 + b\omega_2 \mid 0 \le a, b \in \mathbb{R}; a + b \le 1\}. \tag{2}$$

Subsequently we also need the $SU(3)$-weight lattice $P \subset \mathbb{R}^2$ and its positive chamber $P^+ \subset P$, which are formed by the integer linear combinations

$$P = \{a\omega_1 + b\omega_2 \mid a, b \in \mathbb{Z}\}, \tag{3}$$

$$P^+ = \{a\omega_1 + b\omega_2 \mid a, b \in \mathbb{Z}^{\ge 0}\}. \tag{4}$$

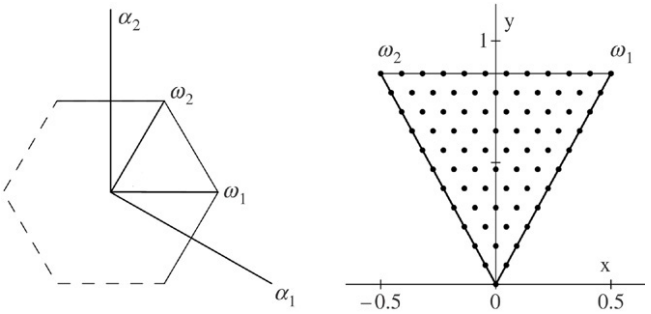

Fig. 1. a (left panel): Representation of the maximal torus T (hexagon) of the $SU(3)$ group in the plane $(x + y + z) = 0$, simple roots α_1 and α_2 of the group, the fundamental weights ω_1 and ω_2, and the fundamental domain F of $SU(3)$. Note that the sides of T plotted by dashed lines do not belong to T. b (right panel): Representation of elements of finite adjoint order $N = 11$ in the fundamental domain (the big dots).

It is convenient to set for now the square length of vectors of the ω-basis to be

$$\langle \omega_k | \omega_k \rangle = \frac{2}{3}, \quad k = 1, 2.$$

Then the α-basis, called the basis of simple roots of $SU(3)$ shown in Fig. 1, is defined by the condition

$$\langle \alpha_k | \omega_j \rangle = \delta_{k,j}, \quad k = 1, 2. \tag{5}$$

It follows that the matrix of scalar products of simple roots, i.e. the Cartan matrix of Lie theory, for the $SU(3)$ group is

$$C = \big(\langle \alpha_k | \alpha_j \rangle\big) = \begin{pmatrix} 2 & -1 \\ -1 & 2 \end{pmatrix}.$$

Hence, between the two bases, $\omega = (\omega_1, \omega_2)$ and $\alpha = (\alpha_1, \alpha_2)$, we have the matrix relations $\alpha = C\omega$ and $\omega = C^{-1}\alpha$, which it is useful to write explicitly as

$$\alpha_1 = 2\omega_1 - \omega_2, \qquad \alpha_2 = 2\omega_2 - \omega_1, \tag{6}$$

$$\omega_1 = \frac{1}{3}(2\alpha_1 + \alpha_2), \qquad \omega_2 = \frac{1}{3}(2\alpha_2 + \alpha_1). \tag{7}$$

It is also useful to introduce the root lattice Q of $SU(3)$:

$$Q = \{a\alpha_1 + b\alpha_2 \mid a, b \in \mathbb{Z}\}.$$

Three copies of Q form P. More precisely, $P = Q \cup (Q + \omega_1) \cup (Q + \omega_2)$.

2.2. Equidistant grid of points in the fundamental region

Our next task now is to introduce uniform grids of discrete points of any density in F, and explain their relation to Lie group theory. Note that the fundamental region F, being an equilateral triangle, can be used to tile the entire plane by its copies. Therefore any such grid can be extended to a triangular lattice on the entire $\mathbb{R}^2$.

Let $\mathsf{F}_N \subset \mathsf{F}$ denote such a grid (see Fig. 1b), where $N \in \mathbb{Z}^{>0}$ is the number of intervals along each of the 3 sides of F. The density of points in F_N is measured by (inversely proportional to) the total number $M_N \equiv |\mathsf{F}_N|$ of points in the grid, which is

$$M_N = \sum_{j=1}^{N+1} j = \frac{1}{2}(N + 1)(N + 2). \tag{8}$$

The points $z_{k,m} \in \mathsf{F}_N$ are conveniently described in the omega basis through

$$z_{k,m} = \frac{k}{N}\omega_1 + \frac{m}{N}\omega_2, \quad k, m \in \mathbb{Z}^{\geq 0}, k + m \leq N. \tag{9}$$

The relation of these points to $SU(3)$ elements $h(x, y, z)$ of the torus (1) is understood if one transforms $z_{k,m}$ to α-bases using (6), and takes into account the barycentric coordinates (x, y, z) of the simple roots, which are $\alpha_1 = (1, -1, 0)$ and $\alpha_2 = (0, 1, -1)$. This results in the element

$$h_{k,m} = \begin{pmatrix} e^{2\pi i \frac{2k+m}{3N}} & 0 & 0 \\ 0 & e^{2\pi i \frac{m-k}{3N}} & 0 \\ 0 & 0 & e^{-2\pi i \frac{2m+k}{3N}} \end{pmatrix}. \tag{10}$$

An important observation for the theory of discrete transforms on Lie groups is that these elements are of *finite order* (EFO; see [15,16] for details) since $h_{k,m}^{3N} = 1$.

When $z_{k,m}$ is one of the vertices of F, i.e. $(k, m) = (0, 0)$, $(N, 0)$ or $(0, N)$, all three eigenvalues of (10) are the same. When it is on one of the three boundary segments, i.e. either $k = 0$, or $m = 0$, or $k + m = N$, there are two distinct values of exponentials in (10). When $z_{k,m}$ is in the interior of F, there are three distinct exponentials. The number of permutations of the diagonal entries in (10) gives the multiplicity $P_{k,m}$ of the elements in T corresponding to the element $h_{k,m} \in \mathsf{F}_N$. Clearly, for those 3 different cases it is equal to 1, 3, and 6, respectively. Thus one can count the total number N_{tot} of elements in $\mathsf{T}_N \subset \mathsf{T}$ (that results from all elements F_N) by adding up the number of vertices, the number of points on each segment of the boundary, and the points interior to F:

$$N_{\text{tot}} = 1 \times 3 + 3 \times 3(N-1) + 6 \times (N-2)(N-1)/2 = 3N^2.$$

2.3. Weyl group orbits of $SU(3)$

In general, the reflection r_ξ of a point z in a mirror containing the origin and orthogonal to ξ is given by

$$r_\xi z = z - \frac{2\langle z|\xi\rangle}{\langle \xi|\xi\rangle}\xi, \quad z, \xi \in \mathbb{R}^2. \tag{11}$$

In particular, $r_\xi \xi = -\xi$ and $r_\xi r_\xi z = z$. Choosing in place of ξ the simple roots α_1 and α_2, one gets the reflections r_{α_1} and r_{α_2}, which we write as r_1 and r_2 to simplify the notation. Particularly important and often used are the reflections of fundamental weights

$$\begin{aligned} &r_1\omega_1 = \omega_1 - \alpha_1 = \omega_2 - \omega_1 \equiv \omega_3, \\ &r_2\omega_2 = \omega_2 - \alpha_2 = \omega_1 - \omega_2 = -\omega_3, \\ &r_1\omega_2 = \omega_2 \quad \text{and} \quad r_2\omega_1 = \omega_1. \end{aligned} \tag{12}$$

Note that here we introduced an element ω_3 which will be useful later on in Section 3. The Weyl group W of $SU(3)$ is generated by the reflections r_1 and r_2. It is a finite (dihedral) group of order 6. The symbol W_λ denotes the set of all distinct points that are generated from $\lambda \in \mathbb{R}^2$ by W, i.e. it is the Weyl group orbit of λ.

There is a unique element in W_λ with non-negative coordinates in the ω-basis. Therefore, if not mentioned otherwise, in the following we use the subscript λ implying the element $\lambda = a\omega_1 + b\omega_2 := (a, b)$ with $a, b \in R^{\geq 0}$. Each point $\mu \in \mathbb{R}^2$ belongs to precisely one Weyl group orbit W_λ. Assuming $a, b \in \mathbb{Z}$, we come to the orbits W_λ with $\lambda \in P^+$ (3). All points μ of these orbits cover the entire weight lattice P.

There are four types of Weyl group orbits, the elements of which in the ω-basis are the following:

$$W_{(0,0)} = \{(0, 0)\} \tag{13}$$

$$W_{(a,0)} = \{(a, 0), (-a, a), (0, -a)\} \tag{14}$$

$$W_{(0,b)} = \{(0, b), (b, -b), (-b, 0)\} \tag{15}$$

$$W_{(a,b)} = \{(a, b), (b, -a-b), (-a-b, a), (-a, a+b), (a+b, -b), (-b, -a)\}. \tag{16}$$

Note that the general form (16) formally describes all particular cases of W_λ. It only becomes degenerate for those particular cases, resulting in 2 copies of $W_{(0,b)}$ or $W_{(a,0)}$ if either $a = 0$ or $b = 0$, respectively, and 6 copies of the element $(0, 0)$ if $a = b = 0$.

It is also worth noticing that in the W-orbit (16) the 4th element is the reflection $r_1\lambda$ of the 1st element. All other elements in (16) are found from these two by applying the pairs of reflections $r_{12} := (r_1 r_2)$ or $r_{21} := (r_2 r_1) = r_{12}^2$ to the 1st and the 4th elements in (16), respectively. These represent the orbits V_λ and $V_{r_1\lambda}$ of the even subgroup of the Weyl group for the elements λ and $r_1\lambda$, respectively, which result in rotations at $\pm 120°$ around the point of origin. Writing λ in the α-basis as $\lambda = A\alpha_1 + B\alpha_2$, where

$$A = \frac{2}{3}(2a + b), \qquad B = \frac{2}{3}(2b + a), \tag{17}$$

the W orbit (16) can be presented as $W_\lambda = V_\lambda \cup V_{r_1\lambda}$, where

$$V_\lambda = \{A\alpha_1 + B\alpha_2, (B - A)\alpha_1 - A\alpha_2, -B\alpha_1 - (B - A)\alpha_2\}, \tag{18}$$

$$V_{r_1\lambda} = \{(B - A)\alpha_1 + B\alpha_2, A\alpha_1 - (B - A)\alpha_2, -B\alpha_1 - A\alpha_2\}. \tag{19}$$

The elements of the second subset can also be seen as reflections r_2 of the elements of V_λ, i.e. $V_{r_1\lambda} = V_{r_2\lambda}$. The vector sum of elements in each of (18) and (19) is equal to 0.

The root system Δ containing the simple roots of $SU(3)$ is the W-orbit $W_{(1,1)}$. In ω- and α-bases we have respectively

$$\Delta := W_{(1,1)} = \{\pm(1, 1), \pm(2, -1), \pm(-1, 2)\} = \{\pm(\alpha_1 + \alpha_2), \pm\alpha_1, \pm\alpha_2\}.$$

In addition to the finite Weyl group of $SU(3)$ generated by the reflections (11), we introduce a larger, affine group $W^{\mathrm{aff}} \supset W$ generated by all affine reflections $R_{K\gamma}$:

$$R_{K\gamma} z := r_\gamma z + K\gamma, \quad z \in \mathbb{R}^2,\ \gamma \in \Delta,\ K \in \mathbb{Z}. \tag{20}$$

Here r_γ is the reflection (11) in the hyperplane orthogonal to the root $\gamma \in \Delta$ and passing through the origin. In $R_{K\gamma}$ it is combined with an additional shift by $K\gamma$, an element of the root lattice Q. More generally we have translations

$$\begin{aligned} r_\gamma R_{K\gamma} z &= r_\gamma(r_\gamma z + K\gamma) = r_\gamma^2 z + K r_\gamma \gamma = z - K\gamma \\ R_{K\gamma} r_\gamma z &= R_{K\gamma}(r_\gamma z) = r_\gamma^2 z + K\gamma = z + K\gamma. \end{aligned} \tag{21}$$

Our interest in the affine Weyl group of $SU(3)$ stems from the properties of orbit functions whose arguments are related by transformations from W^{aff}. Note that r_1 and r_2 formally correspond to reflections in the mirrors containing fundamental weights ω_2 and ω_1, respectively. Choosing $\gamma = \alpha_1 + \alpha_2$ and $K = 1$, we find that the reflection of any $z \in \mathsf{F}$ in the third side of the fundamental triangle F is the affine reflection $R_{\alpha_1+\alpha_2}(z)$.

2.4. Orbit function of $SU(3)$

We are now in a position to define [15,16] an $SU(3)$-orbit function $\Omega_\lambda \equiv \Omega_{a,b}$:

$$\Omega_\lambda(z) := \sum_{\mu \in W_\lambda} \mathrm{e}^{2\pi \mathrm{i}\langle \mu | z\rangle}, \quad z \in \mathbb{R}^2. \tag{22}$$

Note that orbit functions are continuous complex-valued functions, and have continuous derivatives of any order in the entire $\mathbb{R}^2$.

In what follows, the functions $\Omega_\lambda(z)$ are exploited extensively. Therefore it is useful to write them down in detail. The explicit expression of $\Omega_\lambda(z)$ formally depends on the basis one uses for weights $\mu \in W_\lambda$ and for variable z in computing the scalar product $\langle \mu \mid z\rangle$ in (22). Let $\lambda = a\omega_1 + b\omega_2$ and $z = \theta_1\omega_1 + \theta_2\omega_2$, where $\theta_1, \theta_2 \in \mathbb{R}$. Then for the 4 particular types of Weyl group orbits one has the following:

$$\Omega_{0,0}(z) = 1 \tag{23}$$

$$\Omega_{a,0}(z) = \mathrm{e}^{\frac{2\pi \mathrm{i}}{3}a(2\theta_1+\theta_2)} + \mathrm{e}^{\frac{2\pi \mathrm{i}}{3}a(-\theta_1+\theta_2)} + \mathrm{e}^{\frac{2\pi \mathrm{i}}{3}a(-\theta_1-2\theta_2)} \tag{24}$$

$$\Omega_{0,b}(z) = \mathrm{e}^{\frac{2\pi \mathrm{i}}{3}b(\theta_1+2\theta_2)} + \mathrm{e}^{\frac{2\pi i}{3}b(\theta_1-\theta_2)} + \mathrm{e}^{\frac{2\pi i}{3}b(-2\theta_1-\theta_2)} \tag{25}$$

$$\Omega_{a,b}(z) = e^{\frac{2\pi i}{3}[(2a+b)\theta_1+(a+2b)\theta_2]} + e^{\frac{2\pi i}{3}[(-a+b)\theta_1-(2a+b)\theta_2]} + e^{\frac{2\pi i}{3}[(2a+b)\theta_1+(a-b)\theta_2]} + e^{\frac{2\pi i}{3}[(-a+b)\theta_1+(a+2b)\theta_2]} + e^{\frac{2\pi i}{3}[(2a+b)\theta_1+(a-b)\theta_2]} + e^{\frac{2\pi i}{3}[-(a+2b)\theta_1-(2a+b)\theta_2]}. \quad (26)$$

Had we used z in the α-basis, $z = \phi_1\alpha_1 + \phi_2\alpha_2$, we would have in the last (the general) case

$$\Omega_{a,b}(z) = e^{2\pi i[a\phi_1+b\phi_2]} + e^{2\pi i[-a\phi_1+(a+b)\phi_2]} + e^{2\pi i[(a+b)\phi_1-b\phi_2]} + e^{2\pi i[b\phi_1-(a+b)\phi_2]} + e^{2\pi i[(-a-b)\phi_1+(a)\phi_2]} + e^{2\pi i[-b\phi_1-a\phi_2]}. \quad (27)$$

Orbit functions are constituents of characters and have other remarkable properties [20,22]. In special cases they coincide with the characters. More precisely, $\Omega_{1,0}(z)$ and $\Omega_{0,1}(z)$ are the characters of the two 3-dimensional irreducible representations of $SU(3)$; $2 + \Omega_{1,1}(z)$ is the character of the adjoint representation; $\Omega_{2,0}(z) + \Omega_{0,1}(z)$ is the character of one of the 6-dimensional irreducible representations of $SU(3)$, etc. Many more examples are found (in terms of Weyl group orbits) in [8].

Although the method of DOFT is only based on $\Omega_{a,b}(z)$ with integer a and b, it is worth considering the properties of $\Omega_{\alpha,b}$ assuming formally $a, b \in \mathbb{R}$. For the purposes of practical calculations it is also convenient to use further on the general expression (26) for all 4 combinations of a and b. Denoting that function as $\Psi_{a,b}$, we have $\Psi_{a,b} = \Omega_{a,b}(z)$ for $a \neq 0$ and $b \neq 0$, $\Psi_{a,0} = 2\Omega_{a,0}(z)$, $\Psi_{0,b} = 2\Omega_{0,b}(z)$, and $\Psi_{0,0} = 6\Omega_{0,0}(z)$. This renormalized orbit function $\Psi_{a,b}(z) \equiv \Psi_\lambda(z)$ formally represents a continuous function not only of the variable $z \in \mathbb{R}^2$ but also of the second real 2-dimensional variable $\lambda := a\omega_1 + b\omega_2$ over the entire space $\mathbb{R}^2$, *including* the lines corresponding to $a = 0$ or $b = 0$. This is not the case for Ω_λ. This property will be used in the Section 3 below.

For further calculations it is useful to write the explicit expression for Ψ_λ using λ in the α-basis, i.e. $\lambda = A\alpha_1 + B\alpha_2$ where A and B are given by (17). This results in

$$\Psi_{a,b}(z) = e^{2\pi i(A\theta_1+B\theta_2)} + e^{2\pi i((B-A)\theta_1-A\theta_2)} + e^{2\pi i(-B\theta_1-(B-A)\theta_2)} + e^{2\pi i((B-A)\theta_1+B\theta_2)} + e^{2\pi i(A\theta_1-(B-A)\theta_2)} + e^{2\pi i(-B\theta_1-A\theta_2)}. \quad (28)$$

2.5. Symmetry properties

Allowing λ to be in $\mathbb{R}^2$, and not just $\lambda \in P$ of (3), immediately results in the following *scaling* property of orbit functions:

$$\Psi_\lambda(Cz) = \Psi_{C\lambda}(z) \quad \text{for all } C \in \mathbb{R}. \quad (29)$$

This is an obvious consequence of the property $\langle \mu \mid cz \rangle = \langle c\mu \mid z \rangle$ for the scalar product in (22) and of the scalability of the W-orbit $W_{(c\lambda)} = cW_\lambda$.

Symmetry properties of the $SU(3)$ orbit function that involve its complex conjugation and are valid for any $a, b \in \mathbb{R}$ are

$$\Psi_{a,b}(z) = \overline{\Psi_{b,a}(z)}, \quad (30)$$

$$\Psi_{a,b}(z) = \overline{\Psi_{-a,-b}(z)}. \quad (31)$$

Thus, $\Psi_{a,a}(z)$ and the sums $[\Psi_{a,b}(z) + \Psi_{b,a}(z)]$ and $[\Psi_\lambda(z) + \Psi_{-\lambda}(z)]$ all are real-valued functions.

The symmetry properties with respect to the Weyl group which are valid for any $a, b \in \mathbb{R}$ are the following two:

$$\Psi_\lambda(z) = \Psi_{w\lambda}(z) = \Psi_\lambda(wz), \quad (32)$$

$$\Psi_\lambda(z) = \Psi_z(\lambda) \quad \text{for all } z, \lambda \in \mathbb{R}^2. \quad (33)$$

Here w is any sequence of reflection operators r_1 and r_2 which generate the Weyl group W, i.e. $w\lambda = \mu \in W_\lambda$. The property (32) is built into definition (22). The property (33) follows from the observation that the set of 6 scalar products $\{\langle \mu \mid z \rangle \mid \mu \in W_\lambda\}$ coincides with the set $\{\langle \lambda \mid \zeta \rangle \mid \zeta \in W_z\}$, when both W orbits W_λ and W_z are treated in the general form (16).

Fig. 2 shows some examples of $SU(3)$ orbit functions with integer values of a and b. In this case, i.e. when $\lambda \in P$, the orbit functions also are invariant with respect to any root lattice shifts of the argument $z \to z + \xi$, where $\xi \in Q$.

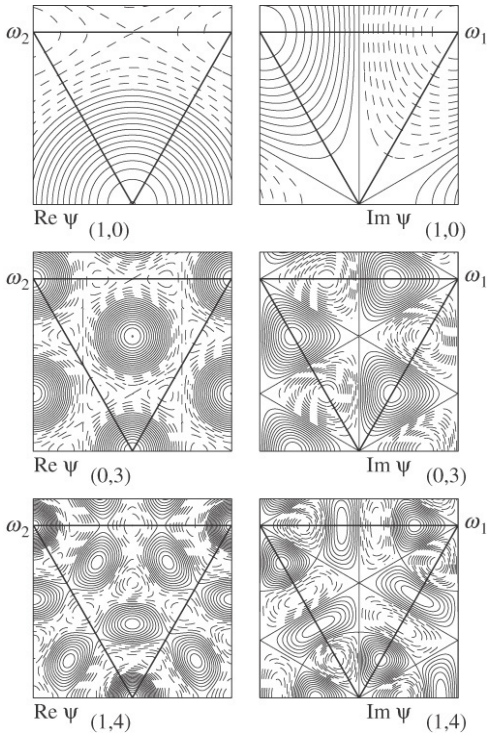

Fig. 2. Orbit functions $\Psi_{a,b}(z)$ for some values of a and b. The dashed contours correspond to negative values of $\Psi_{a,b}(z)$. Note the symmetry of the functions with respect to reflections in each of the 3 sides (solid lines) of the fundamental triangle F.

This is apparent from (27) taking into account that such shifts of z correspond to integer shifts of ϕ_1 and ϕ_2. Therefore in that case we have the symmetry with respect to the affine Weyl group as well:

$$\Psi_\lambda(z) = \Psi_\lambda(R_{n\gamma} z), \quad \text{for } \lambda \in P, n \in \mathbb{Z}, \text{ and } \gamma \in Q. \tag{34}$$

2.6. Orbit functions on F_N

Let us now restrict the continuous variable $z \in \mathbb{R}^2$ to discrete values $z_{k,m} \in \mathsf{F}_N$ given by (9). The orbit function then depends on the vectors $z_{k,m} = \frac{1}{N}(k\omega_1 + m\omega_2) = \frac{1}{N}(k, m)$ and $\lambda = a\omega_1 + b\omega_2 = (a, b)$. Denote the point $z_{a,b} = \frac{1}{N}(a, b)$. It follows from the scaling (29) and the inversion (33) properties that

$$\Psi_{a,b}(z_{k,m}) = \Psi_{k,m}(z_{a,b}). \tag{35}$$

Note that if $a, b \in \mathbb{Z}^{\geq 0}$ and $a + b \leq N$, the point $z_{a,b}$ belongs to the grid F_N.

Example 1. Consider an example $N = 2$. By (8) there are 6 elements in F_2 which correspond to the following:

$$\text{3 vertices of } \mathsf{F}: \quad z_{0,0} = 0, \quad z_{2,0} = \omega_1, \quad z_{0,2} = \omega_2$$

$$\text{midpoints of 3 sides of } \mathsf{F}: \quad z_{1,0} = \frac{1}{2}\omega_1, \quad z_{0,1} = \frac{1}{2}\omega_2, \quad z_{1,1} = \frac{1}{2}\omega_1 + \frac{1}{2}\omega_2.$$

In Table 1 we show several orbit functions evaluated at the points of F_2. There are no points in the interior of F in this case.

By full circles in Fig. 3 we show the points $z_{k,m} \in \mathsf{F}_N$ in the case of $N = 16$. The full triangles correspond to the points $r_1 z_{k,m}$ produced by reflections r_1 of points $z_{k,m}$ in the interior of F_N. These are reflections in the mirror containing the origin and orthogonal to α_1, i.e. along ω_2. The open triangles in Fig. 3 result from the affine reflections $R_{K\gamma} z_{k,m}$ of the inner points of F_N given by (20) where $K = 1$ and $\gamma = \alpha_1 + \alpha_2 \in \Delta$.

Table 1
Values of several $SU(3)$-orbit functions at the six points of F_2 and the multiplicities $P^{[N]}_{k,m}$ (43) for $N = 2$

$z = \frac{1}{2}(k, m)$	(0 0)	$\frac{1}{2}(1, 0)$	$\frac{1}{2}(0, 1)$	$\frac{1}{2}(2, 0)$	$\frac{1}{2}(1, 1)$	$\frac{1}{2}(0, 2)$
$\Psi_{0,0}(z)$	6	6	6	6	6	6
$\Psi_{1,0}(z)$	6	$2\kappa^5$	2κ	$6\kappa^4$	-2	$6\kappa^2$
$\Psi_{0,1}(z)$	6	2κ	$2\kappa^5$	$6\kappa^2$	-2	$6\kappa^4$
$\Psi_{2,0}(z)$	6	$6\kappa^4$	$6\kappa^2$	$6\kappa^2$	6	$6\kappa^4$
$\Psi_{1,1}(z)$	6	-2	-2	6	-2	6
$\Psi_{0,2}(z)$	6	$6\kappa^2$	$6\kappa^4$	$6\kappa^4$	6	$6\kappa^2$
$\Psi_{3,0}(z)$	6	-2	-2	6	-2	6
$\Psi_{2,1}(z)$	6	$2\kappa^5$	2κ	$6\kappa^4$	-2	$6\kappa^2$
$\Psi_{1,2}(z)$	6	2κ	$2\kappa^5$	$6\kappa^2$	-2	$6\kappa^4$
$\Psi_{0,3}(z)$	6	-2	-2	6	-2	6
$\Psi_{2,2}(z)$	6	6	6	6	6	6
$P^{[2]}_{k,m}$	1	3	3	1	3	1

Notation: $\kappa = e^{2\pi i/6}$.

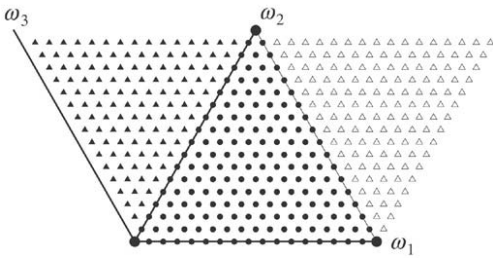

Fig. 3. Elements of finite order for $N = 16$ in the fundamental region (full dots) and in the adjacent triangular regions produced by Weyl group reflections $r_1 z$ (this formally corresponds to reflection in the line of ω_2) shown by full triangles, and the affine reflections $R_\gamma(z)$ (in the line of the third side of F) shown by open triangles. The set composed of F_N (full dots) and full triangles makes H_N, and the union of F_N and open triangles makes the set G_N (see the text).

The values of the orbit function on each of this points can be found from (28) by substituting $\theta_1 = k/N$ and $\theta_2 = m/N$ in the basis (ω_1, ω_2). For practical calculations, like in Section 3 below, sometimes it is useful to express the argument z in the basis (ω_1, ω_3), where $\omega_3 = \omega_2 - \omega_1$ is shown in Fig. 3. For the argument in the latter bases we will use the notation $v_{j,n}$ in order to distinguish it from $z_{k,m} := (k\omega_1 + m\omega_2)/N$ in the basis (ω_1, ω_2). For the same actual point on the grid $z_{k,m} = v_{j,n}$, therefore $k = (j - n)$ and $m = n$. Using this, the orbit function (28) can be rewritten as

$$\Psi_{a,b}(z_{k,m}) \equiv \Psi_{a,b}(v_{j,n}) = \Lambda_{a,b}(z_{k,m}) + \overline{\Lambda_{b,a}(z_{k,m})}, \tag{36}$$

where $\Lambda_{a,b}(z) \equiv \Lambda_\lambda(z)$ is the orbit function of the even subgroup of the Weyl group for the element $\lambda = a\omega_1 + b\omega_2$. In terms of α-basis for λ it can be written as

$$\Lambda_{a,b}(z_{k,m}) := \sum_{\mu \in V_\lambda} e^{2\pi i \langle \mu | z_{k,m} \rangle} = e^{\frac{2\pi i}{N}(Aj+(B-A)n)} + e^{\frac{2\pi i}{N}((B-A)j-Bn)} + e^{\frac{2\pi i}{N}(-Bj+An)}. \tag{37}$$

Here A and B given by (17) are the coordinates of λ in the α-basis, $j = k + m$ and $n = m$. The function $\Lambda_{a,b}$ given by (37) is based on the subset V_λ of half of the elements of W_λ, whereas $\overline{\Lambda_{b,a}}$ is based on the remaining triplet of elements given by (19).

Representation of the grid points in the basis (ω_1, ω_3) allows us to describe the set of points shown in Fig. 3 by full circles ('dots') and full triangles as

$$\left\{ v_{j,n} = \frac{j}{N}\omega_1 + \frac{n}{N}\omega_3 \mid 1 \le j \le N, 0 \le n \le N - 1 \right\}, \tag{38}$$

plus the points $v_{0,0} = 0$ and $v_{N,N} = \omega_2$. We will refer to it as the set H_N. In this basis the points of the grid F_N correspond to $n \leq j$.

Finally, let us write explicit expressions for the orbit function $\Psi_{a,b}(z)$ for all $z \in \mathbb{R}^2$ in terms of Cartesian coordinates x, y. Choose the coordinate system with the y-axis passing symmetrically with respect to fundamental weights ω_1 and ω_2 (i.e. which is bisecting F in Fig. 1), the x-axis passing through the origin, and with the length scale unit equal to the length of the fundamental weights, i.e. $|\omega_1| = |\omega_2| = 1$. The unit vectors e_x and e_y in the directions of the axes x and y, respectively, can be expressed as the vector sums $e_x = \omega_1 - \omega_2$ and $e_y = \frac{1}{\sqrt{3}}(\omega_1 + \omega_2)$, respectively. Then the real and imaginary parts of the orbit functions of $SU(3)$ can be reduced to:

$$\begin{aligned}\operatorname{Re}\Psi_{a,b}(x,y) &= 2\cos\left(2\pi y\frac{a+b}{\sqrt{3}}\right)\cos\left(2\pi x\frac{a-b}{3}\right) + 2\cos\left(2\pi y\frac{a}{\sqrt{3}}\right)\cos\left(2\pi x\frac{2b+a}{3}\right)\\ &\quad +2\cos\left(2\pi y\frac{b}{\sqrt{3}}\right)\cos\left(2\pi x\frac{2a+b}{3}\right). \qquad (39)\\ \operatorname{Im}\Psi_{a,b}(x,y) &= 2\cos\left(2\pi y\frac{a+b}{\sqrt{3}}\right)\sin\left(2\pi x\frac{a-b}{3}\right) + 2\cos\left(2\pi y\frac{a}{\sqrt{3}}\right)\sin\left(2\pi x\frac{2b+a}{3}\right)\\ &\quad -2\cos\left(2\pi y\frac{b}{\sqrt{3}}\right)\sin\left(2\pi x\frac{2a+b}{3}\right). \qquad (40)\end{aligned}$$

3. $SU(3)$ group transform on a triangular grid

In this section we specialize the general results of [16] to the case of $SU(3)$ using also [17].

Consider a function $f_{k,m} := f(z_{k,m})$ given by its values on the points $z_{k,m} \in \mathsf{F}_N \subset F$ of the equilateral triangular grid (9). As defined in [17], a discrete transform of a class function on a semisimple compact Lie group, here $SU(3)$, corresponds to decomposition of this function into a finite series of orbit functions of the group evaluated at the same points F_N:

$$f(z_{k,m}) = \sum_{j,n\geq 0}^{j+n\leq N} C_{jn}\,\Psi_{jn}(z_{km}) \quad \text{for } 0 \leq k, m, k+m \leq N. \qquad (41)$$

This is a system of $|\mathsf{F}_N|$ linear equations with respect to unknown coefficients C_{jn}, each involving (*evaluated at*) a distinct point $z_{k,m}$. The number of terms in the series coincides with $|\mathsf{F}_N|$ of (8). Thus, the Fourier transform of (41) consists in finding the coefficients C_{jn}. That is accomplished in (59) below.

The crucial property that allows realization of such inversion is the discrete pairwise orthogonality (54) of orbit functions Ψ_λ with different λ. A general proof of this property for orbit of compact Lie groups is found in [17]. This tells us that two orbit functions are orthogonal on the set of points F_N if they are separated on F_N. Here we will derive the necessary and sufficient condition for the separability in the case of $SU(3)$. This will make clear the procedure for construction of maximal sets (53) of pairwise orthogonal orbit functions. A by-product of this method is the orthogonality property of the triplets $\Lambda_{a,b}(z)$ (37) that represent orbit functions for the even subgroup of the Weyl group.

3.1. Orthogonality of orbit functions on F_N

A sesquilinear product of two discrete class functions $f(z_{k,m})$ and $g(z_{k,m})$, with $z_{k,m} \in \mathsf{F}_N$, has been defined in [15,16] as follows:

$$\langle f, g\rangle_N := \sum_{z_{k,m}\in T_N} f(z_{k,m})\overline{g(z_{k,m})} = \sum_{z_{k,m}\in \mathsf{F}_N} P_{k,m} f(z_{k,m})\overline{g(z_{k,m})}, \qquad (42)$$

where $P_{k,m}$ is the multiplicity factor

$$P_{k,m} = \begin{cases} 1 & \text{for } k = m = 0, \text{ or } k = N, m = 0, \text{ or } k = 0, m = N \\ 3 & \text{for } 0 < k < N, m = 0, \text{ or } 0 < m < N, k = 0 \text{ or } k, m \neq 0, k + m = N \\ 6 & \text{otherwise.} \end{cases}$$

It corresponds to the number of points in T_N that would belong to the Weyl group orbit of the given point $z_{k,m} \in \mathsf{F}_N$. Equivalently,

$$P_{k,m} = \frac{6}{(1+\delta_{k+m,0})(1+\delta_{k,0}+\delta_{m,0})} \tag{43}$$

where the indices in the Kronecker symbols are read modulo N, i.e. $\delta_{N,0} = \delta_{0,0} = 1$. The transition in (42) from the sum over the points of T_N to the points only of F_N is possible because the class functions are symmetric with respect to Weyl group reflections. Note that this is not the case for triplet functions Λ_λ. The symmetry of these functions only allows transition ('folding') from the set T_N to the set H_N defined above in (38) (and shown in Fig. 3).

The proof of the orthogonality property of orbit functions is based on the decomposition of the product of orbit functions into the sum of orbit functions as described in [17]. This property acquires a very simple form in terms of renormalized orbit functions Ψ_λ instead of Ω_λ.

The product of a pair of renormalized orbit functions Ψ_{λ_1} and Ψ_{λ_2} is reduced to the sum of 6 orbit functions as follows:

$$\Psi_{\lambda_1}(z)\,\Psi_{\lambda_2}(z) = \sum_{\mu_2 \in W_{\lambda_2}} \Psi_{\lambda_1+\mu_2}(z), \tag{44}$$

i.e. where $\mu_2 \in W_{\lambda_2}$ runs over 6 elements of the Weyl orbit of λ_2 in its generalized (degenerate) form of (16).

The proof of this property is straightforward. Take into account that the product of two Ψ-functions represents a sum of 36 exponentials $\mathrm{e}^{2\pi \mathrm{i}\langle \mu_1+\mu_2|z\rangle}$, where $\mu_1 \in W_{\lambda_1}$ and $\mu_2 \equiv \mu_p \in W_{\lambda_2}$. The corresponding 36 sums $(\mu_1+\mu_2)$ can be grouped as follows. Construct the first 6 sums Δ_p fixing μ_1 on some $\lambda_1 \in W_{\lambda_1}$, i.e. $\Delta_p = \lambda_1 + \mu_p$, $p = 1, \ldots, 6$. All remaining sums are produced by 5 consecutive actions of the Weyl group reflections r_1 and r_2 on both λ_1 and μ_p. This results in 6 generalized Weyl group orbits in the form of (16), and hence 6 renormalized orbit functions $\Psi_{\lambda_1+\mu_2}$. ■

Obviously, one can also permute the vectors λ_1 and λ_2 in (44) to choose $\lambda_2 + \mu_1$ with $\mu_1 \in W_{\lambda_1}$. This can only lead to the very same 6 orbit functions, although the indices formally could be different. In practice it might prove useful to choose the longest from the two vectors as λ_1, i.e. $|\lambda_1| \geq |\lambda_2|$.

Note that while both $\lambda_1 \in \mathbb{R}^2$ and $\lambda_2 \in \mathbb{R}^2$ could be chosen from the positive quadrant in the (ω_1, ω_2)-basis, the sums $\Delta_p = \lambda_1 + \mu_2$, $p = 1, \ldots, 6$, could generally have positive and negative indices in that bases. Using (32), in these cases one might want to rewrite the functions Ψ_{Δ_p} as Ψ_{λ_p}, such that λ_p would have both of those indices non-negative. In particular cases some of those 6 functions Ψ_{Δ_p} in (44) might occasionally coincide if relevant elements Δ_p were to belong to the same Weyl group orbit W_{λ_p}.

Let us write these 6 elements Δ_p explicitly for $\lambda_1 = (c, d)$ and $\lambda_2 = (a, b)$. Using (16), we find

$$\begin{aligned}\{\Delta_p\} := \{&(c+a, b+d), (c+b, d-a-b), (c-a-b, d+a),\\ &(c-a, d+a+b), (c+a+b, d-b), (c-b, d-a)\}.\end{aligned} \tag{45}$$

Example 2. On the basis of (45)

$$\Psi_{1,1}\,\Psi_{1,1} = \Psi_{2,2} + \Psi_{3,0} + \Psi_{0,3} + \Psi_{2,-1} + \Psi_{-1,2} + \Psi_{0,0}.$$

Since both $\Psi_{2,-1}$ and $\Psi_{-1,2}$ are equal to $\Psi_{1,1}$, we have

$$\Psi_{1,1}\,\Psi_{1,1} = \Psi_{2,2} + \Psi_{3,0} + \Psi_{0,3} + 2\,\Psi_{1,1} + \Psi_{0,0}.$$

In terms of the original orbit functions Ω_λ this can be rewritten as

$$\Omega_{1,1}\,\Omega_{1,1} = \Omega_{2,2} + 2\Omega_{3,0} + 2\Omega_{0,3} + 2\Omega_{1,1} + 6\Omega_{0,0}.$$

It has been shown in [17] that two orbit functions Ω_{λ_1} and Ω_{λ_2} are orthogonal to each other on F_N if they are separable on F_N. The latter means that $\Omega_{\lambda_1}(z_{k,m}) \neq \Omega_{\lambda_2}(z_{k,m})$ at least at one point $z_{k,m} \in \mathsf{F}_N$. The necessary and sufficient condition for separability of orbit functions, however, has not been specified. Here we provide a complete proof for the discrete orthogonality of orbit functions in the case of $SU(3)$. It therefore also helps to specify the condition of separability of orbit functions.

Proposition 1. *The sesquilinear product of 2 orbit functions*

$$\langle \Psi_{\lambda_1} \mid \Psi_{\lambda_2} \rangle_N = 0 \tag{46}$$

where $\lambda_1, \lambda_2 \in P$, iff the affine Weyl orbits of elements λ_1/N and λ_2/N are different.

In other words this means that a pair of orbit functions corresponding to $\lambda_1 = a_1\omega_1 + b_1\omega_2$ and $\lambda_2 = a_2\omega_1 + b_2\omega_2$ with integer values of a_1, a_2, b_1 and b_2 are orthogonal to each other on the grid F_N (or equivalently T_N), if and only if none of 6 elements $\nu_p \in W_{(\lambda_2/N)}$ in the Weyl orbit of $\frac{1}{N}\lambda_2$ can be connected with the element $\nu_1 := \frac{1}{N}\lambda_1$ by a vector $\Delta_p = \nu_1 - \nu_p$ that would belong to the root lattice Q.

Note that $\overline{\Psi_{\lambda_2}} = \Psi_{-\lambda_2}$. Therefore it follows from (42) and (44) that

$$\langle \Psi_{\lambda_1} \mid \Psi_{\lambda_2} \rangle_N = \sum_{p=1}^{6} \left(\sum_{z_{k,m} \in \mathsf{F}_N} P_{k,m}\, \Psi_{\Delta_p}(z_{k,m}) \right), \tag{47}$$

where $\Delta_p := \lambda_1 - \mu_p$ with $\mu_p \in W_{\lambda_2}$.

Let $\Delta_p = a\omega_1 + b\omega_2$ in ω-basis, or $\Delta_p = A\alpha_1 + B\alpha_2$ in the α-basis with (A, B) given by (17). Because of symmetry property (32), we have

$$\sum_{z_{k,m} \in \mathsf{F}_N} P_{k,m}\, \Psi_{\Delta_p}(z_{k,m}) = \sum_{z_{k,m} \in \mathsf{H}_N} L_{k,m}\, \Psi_{\Delta_p}(z_{k,m}) \tag{48}$$

where the set H_N includes $z_{k,m} \in \mathsf{F}_N$ and the r_1-reflections of points $z_{k,m}$ interior to F (see Fig. 3). Then the new multiplicity factor $L_{k,m} = 3$ for all points $z_{k,m} \in \mathsf{H}_N$, except for the 3 vertices of F where $L_{k,m} = 1$. For each of 6 exponentials in the function Ψ_{Δ_p}, the sum over H_N is then reduced to the product of 2 geometric series, if the argument is transformed into the basis (ω_1, ω_3) as $z_{k,m} = v_{j,n} := (j\omega_1 + n\omega_3)/N$, with $k = (j - n)$ and $m = n$ and one takes care of the 3 vertices 0, ω_1 and ω_2 in the sum. Thus, for the first exponential term in the triad (37) we have

$$\begin{aligned}\sum_{z_{k,m} \in \mathsf{H}_N} L_{k,m} \mathrm{e}^{\frac{2\pi \mathrm{i}}{N}(Aj+(B-A)n)} &= 3\sum_{j=1}^{N} \mathrm{e}^{\frac{2\pi \mathrm{i}}{N}Aj} \sum_{n=0}^{N-1} \mathrm{e}^{\frac{2\pi \mathrm{i}}{N}(B-A)n} + 1 + \mathrm{e}^{2\pi \mathrm{i}B} - 2\mathrm{e}^{2\pi \mathrm{i}A} \\ &= 3\frac{\mathrm{e}^{\frac{2\pi \mathrm{i}}{N}A}(\mathrm{e}^{2\pi \mathrm{i}A} - 1)(\mathrm{e}^{2\pi \mathrm{i}(B-A)} - 1)}{(\mathrm{e}^{\frac{2\pi \mathrm{i}}{N}A} - 1)(\mathrm{e}^{\frac{2\pi \mathrm{i}}{N}(B-A)} - 1)} + 1 + \mathrm{e}^{2\pi \mathrm{i}B} - 2\mathrm{e}^{2\pi \mathrm{i}A}.\end{aligned}$$

The triplet of exponents (37) results in the sum

$$\begin{aligned}\sum_{z_{k,m} \in \mathsf{H}_N} L_{k,m} \Lambda_{\Delta_p}(z_{k,m}) &= 2[\cos 2\pi \mathrm{i}A + \cos 2\pi \mathrm{i}B + \cos 2\pi \mathrm{i}(B - A)] \\ &\quad + \frac{6}{\sigma}\Big[\mathrm{e}^{\frac{2\pi \mathrm{i}}{N}A}(\mathrm{e}^{-\frac{2\pi \mathrm{i}}{N}B} - 1)\cos 2\pi \mathrm{i}B - \mathrm{e}^{\frac{2\pi \mathrm{i}}{N}B}(\mathrm{e}^{-\frac{2\pi \mathrm{i}}{N}A} - 1) \\ &\quad \times \cos 2\pi \mathrm{i}A + (\mathrm{e}^{-\frac{2\pi \mathrm{i}}{N}A} - \mathrm{e}^{-\frac{2\pi \mathrm{i}}{N}B})\cos 2\pi \mathrm{i}(B - A)\Big],\end{aligned} \tag{49}$$

where

$$\sigma = \mathrm{e}^{\frac{2\pi \mathrm{i}}{N}A} - \mathrm{e}^{-\frac{2\pi \mathrm{i}}{N}A} + \mathrm{e}^{-\frac{2\pi \mathrm{i}}{N}B} - \mathrm{e}^{\frac{2\pi \mathrm{i}}{N}B} + \mathrm{e}^{\frac{2\pi \mathrm{i}}{N}(B-A)} - \mathrm{e}^{-\frac{2\pi \mathrm{i}}{N}(B-A)}. \tag{50}$$

For $a, b \in \mathbb{Z}$ the sums $A+B = a+b$, $2A-B = a$ and $2B-A = b$ all are integers. Thus $\mathrm{e}^{2\pi \mathrm{i}A} = \mathrm{e}^{-2\pi \mathrm{i}B} = \mathrm{e}^{2\pi \mathrm{i}(B-A)}$, therefore (49) is reduced to

$$6\cos(2\pi \mathrm{i}A)\left(1 + \frac{1}{\sigma}[\mathrm{e}^{\frac{2\pi \mathrm{i}}{N}(A-B)} - \mathrm{e}^{\frac{2\pi \mathrm{i}}{N}A} + \mathrm{e}^{\frac{2\pi \mathrm{i}}{N}B} - \mathrm{e}^{\frac{2\pi \mathrm{i}}{N}(B-A)} + \mathrm{e}^{-\frac{2\pi \mathrm{i}}{N}A} - \mathrm{e}^{-\frac{2\pi \mathrm{i}}{N}B}]\right) = 0.$$

The derivation of (49) has in fact assumed that neither of ratios A/N, B/N or $(A - B)/N$ is integer, so that $\sigma \neq 0$. Let us assume that one and only one of these values is integer, say $(A - B) = 0$ modulo N. Because also $A + B$ is integer, it follows then that both A and B are integers. Therefore $\mathrm{e}^{2\pi \mathrm{i}A} = \mathrm{e}^{2\pi \mathrm{i}B} = 1$, and hence each of the **summands** of exponential functions, like (49), is reduced to zero.

Thus, the sum of the triplets (37) on the set of points $z \in \mathsf{H}_N$ is not equal to zero if and only if both A/N and B/N are integer numbers. In that case we simply have

$$\sum_{z_{k,m}\in\mathsf{H}_N} L_{k,m}\Lambda_{\Delta_p}(z_{k,m}) = \sum_{z_{k,m}\in\mathsf{T}_N} \Lambda_{\Delta_p}(z_{k,m}) = 3N_{\mathrm{tot}} = 9N^2. \tag{51}$$

Because $\Psi_{a,b} = \Lambda_{a,b} + \overline{\Lambda_{b,a}}$, this means that $\sum P_{k,m}\Psi_{\Delta_p}(z_{k,m})$ over $z_{k,m} \in \mathsf{F}_N$ is equal to zero iff Δ_p/N does not belong to the root lattice Q, and otherwise it is positive. Then this proves the Proposition. ■

3.2. Orthogonality of $\Lambda_{a,b}z$ on H_N and G_N

The proof of the Proposition 1 given above has actually proved a bit more than that. Namely, it has proved the orthogonality of the even subgroup orbit functions, the triads $\Lambda_{a,b}$ defined through (37), on the set T_N, or equivalently on the set H_N with the multiplicity factor $L_{k,m}$. Note that a decomposition property similar to (47) also holds for the functions $\Lambda_{a,b}(z)$. It can be formulated as follows:
The product of two triplet functions Λ_{λ_1} and Λ_{λ_2} is reduced to the sum of 3 orbit functions as follows:

$$\Lambda_{\lambda_1}(z)\Lambda_{\lambda_2}(z) = \sum_{p=1}^{3} \Lambda_{\Delta_p}(z), \tag{52}$$

where $\Delta_p = \lambda_1 + \mu_p$, and the vector $\mu_p \in V_{\lambda_2}$ given by (37).

The discrete orthogonality of functions Λ_λ corresponds to the following proposition:

Proposition 2. *The sesquilinear product of two triplet functions Λ_{λ_1} and Λ_{λ_2} for elements $\lambda_1, \lambda_2 \in P$ is equal to 0 if and only if none of the 3 vectors $\Delta_p = \nu_1 - \nu_p$, where $\nu_1 := \frac{1}{N}\lambda_1$ and $\nu_p \in V_{(\lambda_2/N)}$, belongs to the root lattice Q.*

Note that sesquilinear product of the functions Λ_λ is reduced to the sum over the set H_N,

$$\sum_{z_{k,m}\in T_N} \Lambda_\lambda(z_{k,m})\overline{\Lambda_\beta(z_{k,m})} = \sum_{z_{k,m}\in\mathsf{H}_N} L_{k,m}\Lambda_\lambda(z_{k,m})\overline{\Lambda_\beta(z_{k,m})}.$$

Instead of H_N one can also use the set, call it G_N, which contains F_N and the points of the affine reflections of the inner elements of F_N shown by open triangles in Fig. 3. This is because the points shown in Fig. 3 by full triangles and open triangles are connected by an affine reflection that involves r_{12} and the root lattice shifts on $\gamma = (\alpha_1 + \alpha_2)$, both of which keep Λ_λ invariant (for the standard case $\lambda \in P$).

But the sum over H_N or G_N cannot be further reduced to the points of the triangular grid F_N, because Λ_λ is not generally symmetrical with respect to single reflections r_1 or r_2. In what follows we will limit our consideration to the case of orbit functions Ψ_λ.

3.3. Maximal sets of pairwise orthogonal orbit functions

The inversion of (41), which is our main goal here, is possible due to the following lemma which defines the maximal sets of $M_N = |\mathsf{F}_N|$ functions $\Psi_\lambda(z)$ pairwise orthogonal on the triangular grid, $z \in \mathsf{F}_N$.

Lemma. *The set of orbit functions*

$$\{\Psi_\lambda(z) \mid \lambda = k\omega_1 + m\omega_2, k, m \geq 0;\ k + m \leq N\} \tag{53}$$

represents a maximal set of orbit functions which are pairwise orthogonal with respect to the product (42) for a given N. All other maximal sets $\{\Psi_{\lambda_j}\}$ are found by replacements of any of the Ψ_λ from the set (53) by $\Psi_{\mu+N\xi}$, where $\mu \in W_\lambda$ and ξ is any element in the root lattice Q, which may be different for different λ.

The proof of the Lemma follows directly from Proposition 2. The set of points $\{z_{k,m} = \frac{1}{N}\lambda\}$ corresponding to (53) is exactly the set of EFO in F_N. Since neither of the 2 different elements in T_N could be connected by root lattice shifts $\Delta_p = \xi \in Q$, the pairwise orthogonality of the orbit functions in Eq. (53) is satisfied. On the other hand, addition of any new orbit function Ψ_{k_1,m_1} to the set implies $(k_1 + m_1) > N$. This results in the EFO $z_1 \equiv z_{k_1,m_1}$ of the adjoint order N outside of the fundamental domain, which therefore is conjugate to some element $z_0 \in \mathsf{F}_N$ (see [15]). Hence, $z_1 \in W_{z_0}^{aff}$, and according to Proposition 2, $\langle \Psi_{z_1} \mid \Psi_{z_2} \rangle \neq 0$. ■

3.4. Discrete $SU(3)$ group transform

In this paper we use only the orthogonal sets of orbit functions given by (53) with $\xi = 0$. In that case (42) is written as follows:

$$\langle \Psi_{km} \mid \Psi_{jn} \rangle_N = \delta_{k,j}\delta_{m,n}\langle \Psi_{km} \mid \Psi_{km} \rangle_N = \delta_{k,j}\delta_{m,n}\frac{108N^2}{P_{k,m}}. \tag{54}$$

The proof of Proposition 2 given above suggests that for any $\lambda = k\omega_1 + m\omega_2$ and $\beta = j\omega_1 + n\omega_2$ (which in the general case may not necessarily be in the lattice P^+, but in P) the sesquilinear norm $D = \langle \Psi_\lambda \mid \Psi_\beta \rangle_N$ can be found as follows. Calculate the number J of occurrences of elements $\Delta = \frac{1}{N}(\lambda - \mu)$ and 6 vectors $\mu \in W_\beta$ given by (16), such that $\Delta \in Q$. Each of such cases contributes $6N_{\text{tot}} = 18N^2$ to D (twice the value in (51)), resulting in the total $D = J \times 18N^2$.

In the case of (53) the calculations are straightforward:

$$\langle \Psi_{k,m} \mid \Psi_{k,m} \rangle_N = 18N^2 \times \begin{cases} 6 & \text{for } k = m = 0 \bmod (N) \\ 2 & \text{for } k = 0, 0 < m < N \\ 2 & \text{for } 0 < k < N, m = 0 \\ 2 & \text{for } 0 < k, m, k + m = N \\ 1 & \text{for } 0 < k, m, k + m < N. \end{cases}$$

All these cases are conveniently combined as $J = (1 + \delta_{k+m,0})(1 + \delta_{k,0} + \delta_{m,0}) = 6/P_{k,m}$ resulting in (54).

Example 3. Let us take up the example in Table 1. According to (53), a maximal set of orthogonal orbit functions on F_2 has 6 functions. Among the functions shown in Table 1, one finds for example the following orthogonal sets:

$$\{\Psi_{0,0}, \Psi_{1,0}, \Psi_{0,1}, \Psi_{2,0}, \Psi_{0,2}, \Psi_{1,1}\}; \tag{55}$$
$$\{\Psi_{2,2}, \Psi_{1,0}, \Psi_{0,1}, \Psi_{2,0}, \Psi_{0,2}, \Psi_{1,1}\}; \tag{56}$$
$$\{\Psi_{0,0}, \Psi_{2,1}, \Psi_{0,1}, \Psi_{2,0}, \Psi_{0,2}, \Psi_{0,3}\}; \tag{57}$$
$$\{\Psi_{2,2}, \Psi_{2,1}, \Psi_{1,2}, \Psi_{2,0}, \Psi_{0,2}, \Psi_{3,0}\}. \tag{58}$$

The order of functions in each of these sets is chosen such that it is easy to see which functions from the basic (the first) set can be replaced by which ones from Table 1. Therefore the functions in the same columns above are not orthogonal to each other since they do not satisfy Proposition 2. Thus, the difference between vectors $(3, 0)$ and $(-1, 2) \in W_{(1,1)}$ is exactly $2\alpha_1$; or the elements $(-1, 0) \in W_{(0,1)}$ and $(1, 2)$ can be connected with each other by $\Delta = 2(\alpha_1 + \alpha_2)$.

Example 4. Using the entries of Table 1, let us calculate the products

$$\begin{aligned}
\langle \Psi_{2,0} \mid \Psi_{0,0} \rangle_2 &= \langle \Psi_{0,0} \mid \Psi_{0,2} \rangle_2 = 6(3 + 3 \cdot 3\kappa^4 + 3 \cdot 3\kappa^2 + 3\kappa^2 + 3 \cdot 3 + 3\kappa^4) = 0; \\
\langle \Psi_{1,1} \mid \Psi_{1,2} \rangle_2 &= 6 \cdot 6 - 3 \cdot 2 \cdot 2\kappa^5 - 3 \cdot 2 \cdot 2\kappa + 6 \cdot 6\kappa^4 + 3 \cdot 2 \cdot 2 + 6 \cdot 6\kappa^4 = 0; \\
\langle \Psi_{3,0} \mid \Psi_{1,1} \rangle_2 &= 6 \cdot 6 + 3 \cdot (-2) \cdot (-2) + 3 \cdot (-2) \cdot (-2) + 6 \cdot 6 \\
&\quad + 3 \cdot (-2) \cdot (-2) + 6 \cdot 6 = 144 \ (= 18 \cdot 2^2 \cdot 2).
\end{aligned}$$

A DOFT of a given $\{f_{k,m}\} := \{f(z_{k,m})\}$ corresponds to solving the system of M_N (8) linear equations (41) with respect to M_N variables $C_{j,n}$. Multiply (41) by $P_{k,m}\overline{\Psi_{ps}(z_{k,m})}$, and take the sum over $\{k, m\}$. Applying (54) we find

$$C_{j,n} = \frac{1}{\langle \Psi_{j,n} \mid \Psi_{j,n} \rangle_N} \sum_{k,m \geq 0}^{k+m \leq N} P_{k,m} f_{k,m} \overline{\Psi_{j,n}(z_{k,m})} \tag{59}$$

for all $0 \leq j, n \leq N$.

Equality (59) solves the problem of the DOFT. The set of coefficients $\{C_{k,m} \mid 0 \leq k, m,\ k+m \leq N\}$ represents the discrete Fourier transform of the grid function f_{km} on the orbit functions of the $SU(3)$ group. It is an exact discrete transform. This means that for any set $\{f_{k,m}\}$ resulting from sampling of $f(z)$ at the points $z_{k,m} \in \mathsf{F}_N$ the direct transform $\{C_{k,m}\}$ into the bases of orbit functions $\{\Psi_{k,m}\}$ is uniquely defined by (59). And vice versa, the knowledge of the set $\{C_{k,m}\}$ allows an unambiguous reconstruction of $\{f_{k,m}\}$ as the *inverse* transform (41).

4. Continuous extension of the DOFT

4.1. Generalization of a discrete transform as a continuous function

Let us now consider what happens with a discrete inverse transform (41) if we treat it as a continuous function in the same basis. This means that we allow the argument $z_{k,m}$ of functions in the transform basis, in our case $\Psi_{j,n}(z_{k,m})$, to be continuous $z \in \mathsf{F}$, using the same expansion coefficients $C_{j,n}$ as were calculated for the discrete transform. Obviously, for transforms based on continuous functions the resulting function $\phi(z)$ will be continuous as well. Call it the *continuous extension* (CE) of the (*inverse*) discrete transform. In [3] we have applied this procedure for continuous extension of the DOFT (abbreviated as CEDOFT[2]) in the case of the $SU(2)$ group, and have made a detailed comparison between the properties of CEDOFT and CEDFT for the conventional discrete Fourier transform (DFT; see e.g. [19,18]).

In the case of the $SU(3)$ group considered here, the CEDOFT from $z_{k,m} \in \mathsf{F}_N$ to all points $z \in \mathsf{F}$ is given by the function

$$\phi_N(z) = \sum_{j,n\geq 0}^{j+n\leq N} C_{j,n}\, \Psi_{j,n}(z), \tag{60}$$

where the coefficients $C_{j,n}$ are defined by (59). Obviously, the CEDOFT is exact on the grid, meaning that $\phi(z_{k,m}) = f_{k,m}$ at all points $z_{k,m} \in \mathsf{F}_N$.

In practice one calculates first the DOFT matrix $\{C_{j,n}\}$ to be used further on for calculations of $\phi_N(z)$. But it is useful here to write the expression for $\phi_N(z)$ expressed through the values of $\{f_{k,m}\}$ explicitly. Substituting (59) for $C_{j,n}$ in Eq. (60), we find

$$\phi_N(z) = \frac{1}{108N^2} \sum_{k,m} P_{k,m}\, f_{k,m}\, S_N(z_{x,y}, z_{k,m}). \tag{61}$$

Here $z \equiv z_{x,y} = \frac{1}{N}(x\omega_1 + y\omega_2)$, so that $0 \leq x,\, y,\ (x+y) \leq N$ corresponds to $z \in \mathsf{F}$, and

$$S_N(z_{x,y}, z_{k,m}) = \sum_{j,n\geq 0}^{j+n\leq N} P_{j,n}\, \Psi_{x,y}(z_{j,n})\, \overline{\Psi}_{k,m}(z_{j,n}). \tag{62}$$

Here we have used the symmetry property (35) for the transformation

$$\Psi_{j,n}(z_{x,y})\, \overline{\Psi_{j,n}(z_{k,m})} = \Psi_{x,y}(z_{j,n})\, \overline{\Psi_{k,m}(z_{j,n})}.$$

Note that (62) represents a formal generalization of the sesquilinear product (42) for the case of real $x, y \in \mathbb{R}$. Therefore at any grid point $z_{k,m}$, when $x, y \in \mathbb{Z}^{\geq 0}$, the orthogonality relation (54) can be applied. This immediately confirms the exactness of CEDOFT on the grid, $\phi_N(z_{k,m}) = f_{k,m} \equiv f(z_{j,n})$.

The function $\phi_N(z)$ seems natural to use for interpolation of the given discrete function between the grid points. Take into account that in practical terms the discrete function $\{f_{k,m}\}$ results from the sampling of some continuous function $f(z)$, with $z \in \mathsf{F}$, on the grid points $z_{k,m} \in \mathsf{F}_N$. One can then compare $\phi_N(z)$ of (60) with this model function on the basis of the interpolation error $\varepsilon_N(z) := |\phi_N(z) - f(z)|$. The quality of the interpolation method is defined by the speed of convergence of $\varepsilon_N(z)$ to zero with the increase of N.

4.2. Properties of CEDOFT

A detailed study of CEDOFT on $SU(2)$ group (for 1D functions) made in [3] has shown that its properties are superior to continuous extension of common transforms, in particular of the DFT. Continuous extension of the DFT, which is itself an exact discrete transform on the grid, happens not to converge at all with increase of N. The

[2] Note that earlier in [3,4] we used the acronym DGT, standing for "discrete group transform", and correspondingly CEDGT, instead of DOFT and CEDOFT.

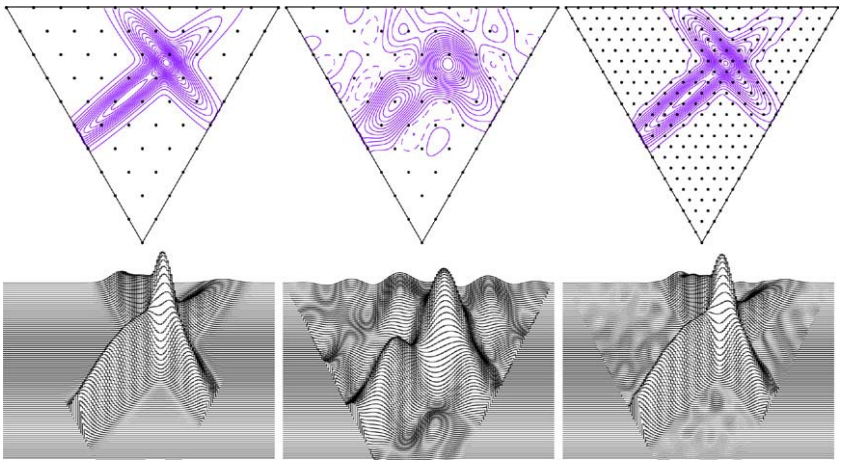

Fig. 4. a (*2 panels on the left*): The contour plot (upper panel) and the 3-dimensional (3-D) image of a model function $f(z)$ composed of a superposition of 2-dimensional Gaussian ellipsoids with the effective widths (dispersions) $\sigma_\perp = 0.03$. The contour lines correspond to separations $\Delta f = 0.1$, and the dashed lines show the negatives contour lines, $\phi(z) < 0$; b (*2 panels in the middle*): A CEDOFT interpolation of the discrete image produced by sampling of the model function on the grid with $N = 20$; c (*2 panels on the right*): CEDOFT approximation of $f(z)$ for a grid with $N = 22$ (see text).

closer the grid points, the faster $\varepsilon(z)$ of CEDFT oscillates, but it does not converge to zero. Various ameliorations of the interpolation behavior have been tried, like "real DFT" (suppressing artificially high-order harmonics), with a problematic success. Oscillations diminish, but the exactness of the transform is destroyed.

Quite different is the behavior of CEDOFT. Its analytic properties proved very similar to the properties of the canonical *continuous* Fourier transform of smooth functions (see e.g. [30,29]). $\varepsilon_N(z)$ rapidly decreases with increasing density of the grid points. In fact, even the partial derivatives of CEDOFT of multi-dimensional *CEDOFT* come very close to $f'(z)$ starting with reasonably dense grids F_N [3]. The CEDOFT also satisfies the *localization principle*. This property ensures that at large N the interpolation quality is defined mainly by the local values of $f_{k,m}$.

Similar are the analytic properties of CEDOFT of $SU(3)$. Discussion and examples of these properties are given in the rest of this section.

4.2.1. Convergence of CEDOFT

In Fig. 4 we show an example of an approximation of a continuous model function $f(z)$ with $z \in \mathsf{F}_N$ (shown in the left panels) by the CEDOFT function $\phi_N(z)$ of the discrete function $f_{k,m} \equiv f(z_{k,m})$ sampled on a grid with $N = 20$.

The function $f(z)$ is composed of the sum of two 2-dimensional Gaussians, with longer axes perpendicular to each other, and with the transverse (to the direction of elongation) dispersions as small as $\sigma_\perp = 0.03$. The 2 panels in the centre show the 3D representation and the contour plot of the $\phi_{10}(z)$ corresponding to the grid with $N = 10$. This function is very far from the original function $f(z)$. This is expected since in that case the grid is very coarse, to catch the width of the Gaussians, $d = tfrac1N \approx 3.3\sigma_\perp$. Surprisingly, however, for a grid with the separation between points d of about $1.5\sigma_\perp$ the amplitude of $\varepsilon(z)$ is already rapidly decreasing. In Fig. 4 the upper and lower panels on the right side show $\phi_{22}(z)$ for $N = 22$. This corresponds to $d \approx 0.45 = 1.5\sigma_\perp$. The difference between the CEDOFT interpolation and $f(z)$ is only noticeable at the lowest contour levels. In the case of Gaussian-type functions there would be no apparent difference between $f(z)$ and its approximation by $\phi(z)$.

Like for the case of the canonical continuous Fourier transform, model functions with larger gradients require denser grids to suppress the high-frequency artifacts (ripples) in the interpolation by the inverse transform. The convergence $\phi_N(z) \to f(z)$ with increasing N remains fast in any case.

4.2.2. Convergence of the truncated CEDOFT

Fig. 5 demonstrates the convergence of CEDOFT for a discrete function $\{f_{k,m}\}$ resulting from the sampling of a model 'table' function in the form $f(z) \propto \mathrm{e}^{(x_1\sigma_1)^4+(x_2/\sigma_2)^4}$ (in terms of Cartesian variables (x_1, x_2) in the plane $z \in \mathbb{R}^2$). Besides that, $\{f_{k,m}\}$ contains a 'hot pixel' from the sampling of a very narrow 2-D Gaussian function centred at some distant point of the grid, and with the same height as the main function. For the chosen model parameters

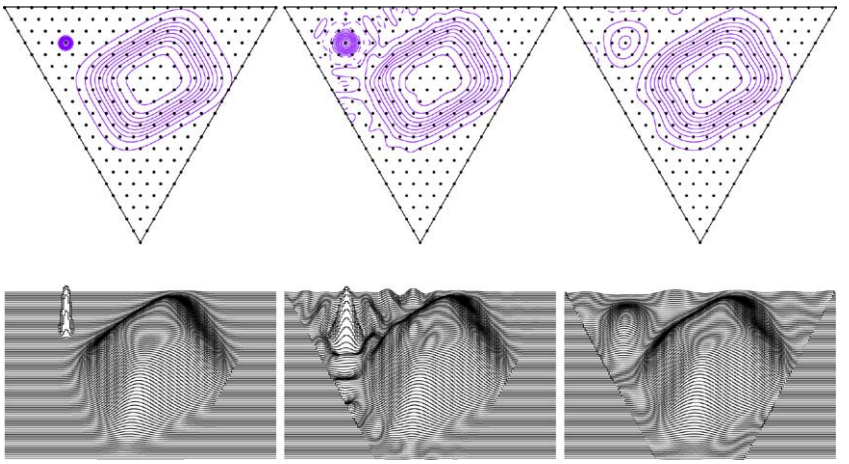

Fig. 5. a (*2 panels on the left*): The contour plot (upper panel) and the 3-dimensional view of a model function composed of 2-dimensional continuous Gaussian ellipsoid, onto which 2 narrow spikes which produce 2 'hot pixels' (after sampling of the analog signal on the grid) are superimposed. The heights of the spikes are equal to half of the height of the ellipsoid; b (*2 panels in the middle*): A direct (i.e. *without filtering*) CEDGT interpolation of the discrete image produced by sampling of the analog image on the grid with $N = 20$; c (*2 panels on the right*): CEDGT view of the image after application of the filter with $C_f = 0.5$ (see the text).

(σ_1, σ_2) the grid with $N = 20$ intervals is sufficiently dense, so that in most parts the model function is approximated by $\phi_N(z)$ sufficiently well. But on the corner closest to the 'hot pixel' the ripples propagating from that 'hot point' are distorting the pattern significantly (two panels in the middle of Fig. 5).

In Fig. 5c (panels on the right) we show the image produced by the truncated CEDOFT function $\tilde{\phi}_{N,M}(z)$. It represents the trigonometric polynomial series (60), where only the terms with $C_{j,n}$ corresponding to the harmonic order $K = (j + n) \leq M$ are preserved, and the others are discarded, i.e. $C_{j,n} \to 0$ for $K > M$. This figure demonstrates that such a truncated CEDOFT series is also converging. The truncated function is no longer exact at the grid points. However, the noise (ripples) from the 'hot pixel' apparent in the exact CEDOFT interpolation $\phi_N(z)$ is essentially suppressed in the area of the main model function. This provides a much better overall approximation to the original function $f(z)$. Furthermore, the value of $\tilde{\phi}_{N,M}(z)$ in the 'hot pixel' itself is essentially suppressed (by a factor of ∼4).

This effect is understood from the analysis of the frequency content of the discrete image $f_{k,m}$ shown in Fig. 6. It shows the mean absolute values of the Fourier coefficients $C_{j,n}$ of harmonic order K. Like for the case of 2-dimensional DCT, in the case of the $SU(3)$ transform the Fourier coefficients of a reasonable image are also concentrated in the domain of lower frequencies. Meanwhile, the coefficients of the DOFT of the 'hot pixel' (i.e. a δ-function), or of any random noise, also represent a random noise (i.e. the analog of a constant). Therefore the noise typically dominates at high frequencies. Discarding high frequencies corresponds effectively to removing the noise by such simple low-pass filtering.

The effectiveness of this approach for data processing has been demonstrated in [4] by application of the $SU(3)$ CEDOFT for the processing images collected by contemporary gamma-ray astronomy detectors which are based on hexagonal symmetry grids.

4.2.3. Localization property

A very important property of the CEDOFT on $SU(3)$, similar to the case for the $SU(2) \times SU(2)$ group DOFT, consists in the validity of the so called *localization principle* (see e.g. [30,29]). This important property implies that variations in the discrete function $\{f_{k,m}\}$ at the points of the grid sufficiently far from the given point $z_{x,y} = \frac{1}{N}(x\omega_1 + y\omega_2)$ do not noticeably change the values of $\phi_N(z)$ in the vicinity of $z_{x,y}$. This can be formulated as follows:

Localization principle: *Let a grid function* $\{f_{k,m} \mid k, m \geq 0, k + m \leq N\}$ *result from a piecewise smooth function* $f(z)$ *limited to the region* $z \in \mathsf{F}$ *sampled on the grid* F_N. *At any given point* $z_{x,y} \in \mathsf{F}$, *and for any small* $d > 0$ *and* $\epsilon > 0$ *there exists a number* $N_d(\epsilon)$ *such that for all* $N > N_d(\epsilon)$ *the continuous extension of the discrete inverse transform* $\phi_N(z)$ *depends within the accuracy* ϵ *only on the values of* $f(z_{k,m})$ *in the d-neighborhood of* $z_{x,y}$, *i.e.:*

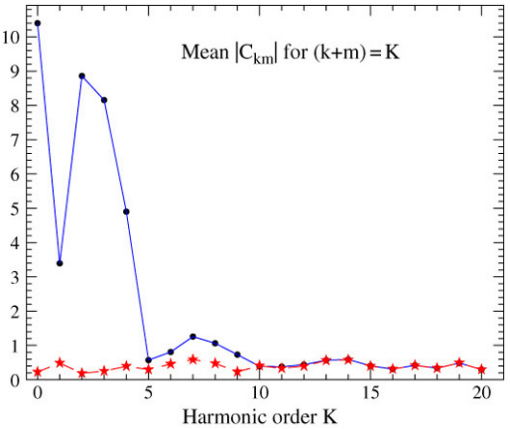

Fig. 6. The averaged absolute values $|C_{k,m}|$ of the DOFT coefficients of the given harmonic order $K = k + m$ (shown by big dots) for the model function of Fig. 5 sampled on the grid with $N = 20$. The stars show the mean values $|C'_{k,m}|$ of the DOFT of the 'hot pixel' alone (see the caption in Fig. 5).

for any $\epsilon > 0$ *and* $d > 0\ \exists\ N_d(\epsilon)$ *such that* $\forall N > N_d(\epsilon) \Longrightarrow$

$$| \phi_N(z_{x,y}) - \frac{1}{108N^2} \sum_{z_{k,m}} P_{k,m;N} f_{k,m} S_N(z_{x,y}, z_{k,m}) | < \epsilon, \tag{63}$$

where the sum is taken only over the values of $\{k, m\}$ *satisfying the condition* $|z_{k,m} - z_{x,y}| < d$.

Recall that at any grid point $z_{x,y} \in \mathsf{F}_N$ the CEDOFT is exact. So it is independent of any other values of the grid function except for $f_{x,y}$. The localization property becomes important for the accuracy of interpolation of the functions between the grid points. In fact, the localization principle tells us that the interpolation provided by CEDOFT trigonometric polynomial $\phi_N(z)$ at some point z is asymptotically independent of the deviations of the values of $\{f_{k,m}\}$ at a distant location, $|z_{k,m} - z| \gg 1/N$. Thus, even high-amplitude random noise in some 'hot pixels' in the real data should have little impact on the CEDOFT interpolation if those pixels are not close to the region of interest. The fast decay of the amplitude of the ripples from the 'hot pixel' in Fig. 5b is the result of the localization property.

Note that the validity of the localization principle effectively means that the sesquilinear product of 2 generalized orbit functions given by (62) with $x, y \in \mathbb{R}$ asymptotically tends to zero for any small but fixed distance $d > 0$ between the arguments in S_N. In other words, in the limit $N \to \infty$ one has

$$S_N(z_{x,y}, z_{k,m}) \to \delta(z_{x,y} - z_{k,m}) \quad \text{for } z_{x,y}, z_{k,m} \in \mathsf{F}. \tag{64}$$

It is clear from (63) if we choose a discrete delta function centred at some $z_0 \equiv (k_0, m_0) \neq z_{x,y}$ (i.e. at a 'hot pixel') for $\{f_{k,m}\}$.

On the other hand, (64) also is a sufficient condition for the proof of (63). Indeed, the number of additions in the sum in (61) corresponding to $f_{k,m}$ outside of a given d-neighborhood of $z_{x,y}$ is increasing $\propto N^2$. This is exactly compensated by the factor $1/N^2$ in (63). Therefore the decline of $S_N(z_{x,y}, z_{k,m})$ in the case of some non-zero distance $d > 0$ between $z_{x,y}$ and $z_{k,m}$ would prove (63). Note that effectively the property (64) corresponds to the known property of orthogonality of the bilinear product of continuous orbit functions in the integral over the region F.

An analytic proof of the localization property has been given for the CEDOFT of the $SU(2)$ group [3]. In the case of $SU(3)$ the mathematical proof is more difficult, and we limit the discussion here to numerical examples of that effect.

4.2.4. Differentiability property

Finally, it is also worth mentioning the convergence of partial derivatives of $\partial\phi_N/\partial z_l$ (in the z_l direction) to the respective derivatives $\partial f/\partial z_l$. The accurate analytic proof of this property in the case of $SU(2)$ is found in [3]. In the case of $SU(3)$ the proof is more problematic, and is also beyond the scope of this paper.

From the perspective of demonstration by numerical computation, the convergence of derivatives is apparent from the excellent interpolation of the model function with $\phi_N(z)$ already on Fig. 4c for a grid with $N = 22$. In the case

of Fig. 5, the derivatives of $\phi_N(z)$ in Fig. 5b and of $f(z)$ shown in Fig. 5a are close to each other over most of the triangular region F, except for the region close to the hot pixel. Here the derivatives of the ripples would dominate the derivatives $\partial\phi_N/\partial z_l$. However, because of the localization property, with further increase of the grid density the region affected by noise from the hot pixel would shrink. Therefore in that limit the derivatives of the model function would be recovered by differentiation of $\phi_N(z)$ over the entire region of the 'table function'

5. Concluding remarks

As a concluding remark, we would like to note that practical computation of the DOFT on $SU(3)$ is sufficiently fast. In principle, it might become even comparable with the speed of DCT/DFT computation if or when the FFT-type algorithms for fast calculations of this transform are developed. The very structure of the orbit functions, representing a combination of complex exponential functions of given harmonic orders like in the case of standard DFT, assumes such a possibility. In any case, this transform compares very favorably with other current techniques for Fourier-type decompositions on hexagonal/triangular grids (see e.g. [14]). Also, realization of the DOFT for other types of triangular symmetries has been considered recently in [24–26]. All of these factors allow practical implementation of methods of Fourier analysis for discrete data formed on detector grids of different triangular and rectangular symmetries, as suggested in [4] for the gamma-ray astronomy data. It is also important that the methods of the DOFT can be also implemented for higher-dimensional grids as well using orbit functions for Lie groups of higher ranks.

Acknowledgements

We acknowledge the partial support of the National Science and Engineering Research Council of Canada, of MITACS, and of NATO. We are also grateful to F.W. Lemire for a number of constructive suggestions and comments.

References

[1] N. Ahmed, T. Natarajan, K.R. Rao, Discrete cosine transform, IEEE Trans. Comput. C-23 (1974) 90–93.
[2] A. Akhperjanian, A. Atoyan, J. Patera, V. Sahakian, Application of multi-dimensional discrete transforms on Lie groups for image processing, in: E. Shahbazian, G. Rogova, P. Valin (Eds.), Data Fusion for Situation Monitoring, Incident Detection, Alert and Response Management, in: NATO Science Series, III, vol. 198, IOS Press, Amsterdam, 2005, pp. 417–425.
[3] A. Atoyan, J. Patera, Properties of continuous Fourier extension of the discrete cosine transform and its multidimensional generalization, J. Math. Phys. 45 (2004) 2468–2491.
[4] A. Atoyan, J. Patera, V. Sahakian, A. Akhperjanian, Fourier transform method for imaging atmospheric Cherenkov telescopes, Astroparticle Phys. 23 (2005) 79–95.
[5] A. Atoyan, J. Patera, Continuous Extension of the Discrete Cosine Transform, and its Applications to Data Processing (Workshop on Group Theory and Numerical Methods, Montreal, 26-31 May, 2003), in: CRM Proceedings and Lecture Notes, vol. 39, 2005, pp. 1–15.
[6] A. Atoyan, J. Patera, Application of continuous extension of DCT to FLIR images, in: E. Shahbazian, G. Rogova, P. Valin (Eds.), Data Fusion for Situation Monitoring, Incident Detection, Alert and Response Management, in: NATO Science Series, III, vol. 198, IOS Press, Amsterdam, 2005, pp. 417–425.
[7] R.N. Bracewell, Numerical transforms, Science (1990) 697–704.
[8] M.R. Bremner, R.V. Moody, J. Patera, Tables of Dominant Weight Multiplicities for Representations of Simple Lie Algebras, Marcel Dekker, New York, ISBN: 0-8247-7270-9, 1985, 340 pages.
[9] S. Grimm, J. Patera, Decomposition of tensor products of the fundamental representations of E_8, in: L. Vinet (Ed.), Advances in Mathematical Sciences – CRM's 25 Years, in: CRM Proc. Lecture Notes, vol. 11, Amer. Math. Soc., Providence, RI, 1997, p. 32.
[10] S. Grim, F.W. Lemire, J. Patera, Discrete group transforms on $SU(2) \times SU(2)$ and $SU(3)$, in: Proc. Conf. on Lie and Jordan Algebras, vol. 6, Resenhas do Instituto de Matematica e Estatistica da Universidade de Sao Paulo, 2004, pp. 199–214.
[11] A. Klimyk, J. Patera, Orbit Functions, in: SIGMA, vol. 2, 2006, Paper 6 (67 pages). math-ph/0601037.
[12] W.G. McKay, R.V. Moody, J. Patera, Tables of E_8 characters and decomposition of plethysms, in: D.J. Britten, F.W. Lemire, R.V. Moody (Eds.), Lie Algebras and Related Topics, Amer. Math. Society, Providence, RI, 1985, pp. 227–264.
[13] W.G. McKay, R.V. Moody, J. Patera, Decomposition of tensor products of E_8 representations, Algebr. Groups Geom. 3 (1986) 286–328.
[14] R.M. Mersereau, The processing of hexagonally sampled two-dimensional signals, Proc. IEEE 67 (1979) 930–949.
[15] R.V. Moody, J. Patera, Elements of finite order in Lie groups and their applications, in: W. Zachary (Ed.), XIII Int. Colloq. on Group Theoretical Methods in Physics, World Scientific Publishers, Singapore, 1984, pp. 308–318.
[16] R.V. Moody, J. Patera, Characters of elements of finite order in simple Lie groups, SIAM J. Algebr. Discrete Methods 5 (1984) 359–383.
[17] R.V. Moody, J. Patera, Computation of character decompositions of class functions on compact semisimple Lie groups, Math. Comput. 48 (1987) 799–827.
[18] H.J. Nussbaumer, Fast Fourier transform and convolution algorithms, Springer-Verlag, Berlin, Heidelberg, New York, 1982.
[19] A.V. Oppenheim, R.W. Schafer, Digital Signal Processing, Prentice-Hall, Englewood Cliffs, 1975.

[20] J. Patera, Orbit functions of compact semisimple Lie groups as special functions, in: Symmetry in Nonlinear Mathematical Physics, in: Proceedings of the Nat. Acad. Sci., vol. 30, Kiev, Ukraine, 2004, pp 1152–1160.
[21] J. Patera, Compact simple Lie groups and their C-, S-, and E-transforms, in: SIGMA, vol. 1, 2005, Paper 25 (6 pages).
[22] J. Patera, Algebraic Solutions of the Neumann Boundary Value Problems on Fundamental Region of a Compact Semisimple Lie Group, (Workshop on Group Theory and Numerical Methods, Montreal, 26–31 May, 2003) in: CRM Proceedings and Lecture Notes, vol. 39, 2005 (in press).
[23] J. Patera, A. Zaratsyan, Discrete and continuous cosine transform generalized to Lie groups $SU(2) \times SU(2)$ and $O(5)$, J. Math. Phys. 46 (2005) 053514.
[24] J. Patera, A. Zaratsyan, Discrete and continuous cosine transform generalized to Lie groups $SU(3)$ and $G(2)$, J. Math. Phys. 46 (2005) 113506.
[25] J. Patera, A. Zaratsyan, Discrete and continuous sine transform generalized to the semisimple Lie groups of rank two, J. Math. Phys. (2006) (in press).
[26] K.R. Rao, P. Yip, Discrete Cosine Transform - Algorithms, Advantages, Applications, Academic Press, 1990.
[27] D. Stranneby, Digital Signal Processing: DSP and Applications, Newnes, Oxford, 2001.
[28] A. Teolis, Computational Signal Processing with Wavelets, Birkhäuser, Boston, 1998.
[29] G.P. Tolstov, Fourier Series, Dover, New York, 1976.
[30] A. Zygmund, Trigonometric Series, Cambridge University Press, 1959.